WiCPD: Wireless Child Presence Detection System for Smart Cars

Xiaolu Zeng, Beibei Wang, *Senior Member, IEEE*, Chenshu Wu, *Senior Member, IEEE*, Sai Deepika Regani, and K. J. Ray Liu, *Fellow, IEEE*

***Abstract*—Child presence detection (CPD) is becoming a regulatory requirement for car manufacturers to save children's lives when they are left alone in unattended vehicles. However, most of the existing solutions require dedicated devices and suffer from limited accuracy and coverage. In this article, we build WiCPD, the first-of-its-kind in-car CPD system using commodity Wi-Fi, which can cover the entire interior of a car with no blind spot. First, we introduce a statistical electromagnetic model which accounts for the impact of motion on all the multipaths inside a car, followed by a motion statistics metric indicating the ambient motion intensity and a signal-to-noise-ratio (SNR) boosting scheme to extract the minute chest movement. Then, we design a unified CPD framework consisting of three target detector modules, including a motion target detector to detect a child in motion/awake, a stationary target detector to detect a stationary/sleeping child, and a transition target detector to detect a sleeping child with sporadic motion who is missed by both the motion and stationary target detectors. We implement a real-time WiCPD system by using commercial Wi-Fi chipsets, deploy it over 20 different cars, and collect data for multiple children aging from 4 to 50 months. The results show that WiCPD can achieve 100% detection rate within 8 s when the child is awake/in-motion and 96.56% detection rate within 20 s for a static/sleeping child. Extensive experiments also demonstrate that WiCPD can be easily deployed in minutes without calibration and enjoys very low CPU and memory consumption, thus promising a practical candidate for CPD applications.**

***Index Terms*—Child presence detection (CPD), in-vehicle sensing, real-time system, smart car, wireless sensing.**

I. Introduction

With the proliferation of automobiles, the heatstroke, and death of children caused by being left alone in a vehicle have gained increasing attention all over the world. According to the *Heat Stress From Enclosed Vehicles* [1], [2], 882 children have died (an average of 38 per year) and many more have suffered disabilities due to organ or brain damages caused by pediatric vehicular heatstroke (PVH) since 1998 in the U.S. As more than 97% of the children reported are under the age of 6 who have little ability to exit the vehicle on his/her own, child presence detection (CPD) is becoming a necessary function to improve the safety of cars, especially in hot weather when the temperature inside a closed car can become fatal within a few minutes. Toward this end, from 2022, the European new car assessment programme (NCAP) will reward solutions of CPD Systems, which are also considered as a regulatory requirement for all newly manufactured passenger vehicles starting from 2023. Equipped with CPD, a child left alone in an unattended car can be detected and caregivers or emergency services will be alerted to avoid heatstroke fatalities [3].

Pioneer efforts have explored CPD based on different techniques/devices as summarized in Table I. Early CPD systems are implemented by leveraging the information from a variety of sensors equipped on the baby seat, such as the optical/weight/heat/pressure sensors [4]–[8]. However, the sensor-based methods have several drawbacks, such as the limited coverage making it hard to detect a child outside the baby seat, high false alarm rate (for example, a child cannot be easily distinguished from an inanimate item of a similar weight using weight sensors), and *ad hoc* parameters corresponding to different children and cars. Later, wireless transceivers [9] and capacitive/electric sensors [10] were introduced to reduce the false alarm rate while the detection area is still limited within/next to the baby seat. Pyroelectric infrared (PIR) sensor-based approaches [11]–[13] turned out to be able to enlarge the coverage by detecting the motion of a child. However, PIR sensors are susceptible to the temperature of the surrounding environment, which degrades its reliability in practice. Vision-based CPD systems [14]–[16] are more reliable in detection accuracy by using image/video processing. However, they usually require dedicated hardware/cameras, thus increasing the cost and energy consumption of the car. Also, the quality of the image/video is vulnerable to light conditions. Although the latest machine learning-based techniques [17] have achieved better detection accuracy, they still heavily depend on the quality of the input image, thus preventing their practical deployments.

Recently, radio frequency (RF) based in-vehicle human sensing has been extensively explored based on vital sign detection [18], [19], location estimation [20]–[25], etc., because of its superiority in preserving privacy and requiring no wearable sensor [26], [27]. However, to detect the subtle motion corresponding to vital signs, such as the

Manuscript received 16 December 2021; revised 3 July 2022; accepted 25 July 2022. Date of publication 29 July 2022; date of current version 7 December 2022. *(Corresponding author: Xiaolu Zeng.)*

Xiaolu Zeng is with the School of Information and Electronics, Beijing Institute of Technology, Beijing 100081, China (e-mail: xlzeng09@bit.edu.cn).

Beibei Wang, Sai Deepika Regani, and K. J. Ray Liu are with Origin Wireless Inc., Greenbelt, MD 20770 USA (e-mail: beibei.wang@originwirelessai.com; deepika.regani@originwirelessai.com; ray.liu@originwirelessai.com).

Chenshu Wu is with the Department of Computer Science, The University of Hong Kong, Hong Kong, China, and also with Origin Wireless Inc., Greenbelt, MD 20770 USA (e-mail: chenshu@cs.hku.hk).

Digital Object Identifier 10.1109/JIOT.2022.3194873

2327-4662 © 2022 IEEE. Personal use is permitted, but republication/redistribution requires IEEE permission.
See https://www.ieee.org/publications/rights/index.html for more information.

Authorized licensed use limited to: University of Maryland College Park. Downloaded on November 25,2024 at 20:18:04 UTC from IEEE Xplore. Restrictions apply.

TABLE I
COMPARISON OF STATE-OF-THE-ART WORKS FOR IN CAR CPD

Methods	Coverage	Low-cost	Calibration-free	Accurate	Responsive
Sensors (weight/pressure) [4]–[10]	Baby seat	✗	✗	✗	Fast[3]
PIR (motion/sensing) [11]–[13]	LoS[1]	✓	✓	✗	Moderate
Vision (image/video) [14]–[16]	LoS	✗	✓	✓	Moderate
Radar (vital sign/motion) [20]–[25]	FoV[2]	✗	✓	✓	Fast
WiCPD (motion/breathing/classifier)[4]	Whole car	✓	✓	✓	$\leq 6/17$s

[1] Line-of-Sight (LoS) [2] File-of-View (FoV) of radar array [3] The CPD system is considered as fast if it can respond within 1 minute while longer 1 minute is called moderate in this paper, which is empirically calculated from in-car temperature rising experiments in [1]. [4] 6s corresponds to awake/motion baby while 17s is for sleeping/stationary baby, with detection rate $\geq 95\%$.

chest movement (4–12 mm) and heartbeat displacement (0.2–0.5 mm) and then identify the presence of a human, most of them [20]–[25] rely on the millimeter-Wave (mmWave) signal, which is not readily available inside most vehicles nowadays.

While many works have been proposed on realizing CPD, to the best of our knowledge, none of the existing technology is ready for world-wide deployment which should ideally satisfy the following requirements.

1) *Accurate:* It should be sensitive enough to achieve near 100% detection rate as every miss detection may become catastrophic. Accompanied with the high sensitivity is a potentially escalated false alarm rate, yet it does not take much effort for parents/caregivers to turn off the false alarm alert while rest assured the child is better protected, if the false alarm rate is reasonably low.
2) *Responsive:* It should be responsive to the presence of a child (if any) for two main reasons. First, an ambient temperature of 22 °C (73 °F) in a closed car can drive up at 3.47 °C (6.25 °F) per 5 mins [1], [28] and heat exhaustion can begin 40 °C and over 54 °C often leads to heatstroke [29]. In addition, parents/caregivers would like to receive alerts as early as possible before they walk too far away from the car.
3) *Large Coverage:* It should be able to cover the entire interior of a car with no blind spot, including both on and under the seat, since a child may fall on the footwell areas when he/she is struggling.
4) *Calibration Free:* It is expected to work robustly for different car models, children of different ages/genders/weights in all weather/temperature/environments without calibration.
5) *Low Cost:* Installation of the CPD should require very low efforts, and ideally, it should reuse the current in-car facilities with no additional hardware change.

With the ubiquitous deployment of Wi-Fi in the era of the Internet of Things (IoT), it is shown that about 12%–33% (*varies in different regions*) of the vehicles in operation worldwide already have Wi-Fi and more (*about 400 million by 2025* [30]–[34]) are planning to have Wi-Fi equipment. As a result, many in-vehicle Wi-Fi sensing-based functionalities have emerged, such as driver's activity monitoring [35], emotion sensing [36], etc., to improve the driving safety by reusing the in-car Wi-Fi equipment. Therefore, we ask the following question: *Can we use Wi-Fi sensing to do CPD?* Although the Wi-Fi sensing technology has driven many practical in-vehicle applications [35]–[39], enabling CPD using commercial Wi-Fi while satisfying all the five aforementioned requirements entails several challenges.

First, while the existing works have shown the feasibility of using the variation of the wireless signal [40] to detect an adult [41], the size of a child is much smaller than an adult and his/her motion/breathing strength is much weaker as well. Thus, a child causes much weaker impact on the wireless signal than an adult, making him/her more challenging to be detected. mmWave-based methods [21]–[25] are demonstrated to be able to capture both the activity motion (head/arm/torso movement) and breathing motion (chest movement of a stationary child) due to its short wavelength and larger bandwidth. However, the coverage of mmWave-based methods is limited within the Field-of-View (FoV) with respect to corresponding mmWave radar.

Second, it is nontrivial to achieve a fast response in CPD. Although existing motion detector [40], [41] can work in general motion sensing applications, most of them rely on a change detection of the channel profile, e.g., variance, phase difference, etc. Since they do not leverage the reflection signal from all the dynamic scatters constructively, most of them require a long window of samples and thus causing a large detection delay. For example, DeMan [41] requires 500 packets (i.e., about 17 s corresponding to a sample rate of 30 Hz) to achieve 98% detection rate for an adult in motion. Even longer detection delays are expected in detecting a child, due to his/her much smaller size and weaker motion strength than an adult.

To tackle these challenges, we consider a statistical electromagnetic (EM) model [42], which calculates the autocorrelation function (ACF) of the channel state information (CSI) measurements consisting of all the multipath components. Then, a motion statistics metric is elaborated to quantify the intensity of ambient motion, which can ensure that each dynamic scatterer, regardless of its location, contributes to the overall motion statistics constructively. However, in most of the conventional variation-based methods, the dynamic scatterers in different locations may contribute to the CSI variation destructively. As a result, our motion detection is more sensitive than most of the conventional variation-based approaches [40].

Authorized licensed use limited to: University of Maryland College Park. Downloaded on November 25,2024 at 20:18:04 UTC from IEEE Xplore. Restrictions apply.

To detect a child accurately regardless of his status, i.e., motion/awake, stationary/sleeping or in between (sleeping with occasional motion), three target detectors are designed: 1) a *motion target detector* to detect a child who is in motion/awake based on the motion statistics; 2) a *stationary target detector* to identify a stationary child who has very few motions such as when he/she is in sleeping. We consider a maximal ratio combining (MRC) [43] scheme to improve the signal-to-noise-ratio (SNR) of the ACF using the motion intensity in each subcarrier as the channel gain. The boosted ACF is then leveraged to extract the minute breathing pattern/chest movement and estimate the breathing rate of the child [44]. Then, we devise a module to check if a continuous breathing rate can be detected and the breathing rate should fall within a normal range of a child for stationary child detection; and 3) a naive Bayes classifier-based *transition target detector* to deal with the case when the motion and stationary target detectors fail to detect a child in transition status. For example, a sleeping child may have minor motion, such as subtle head rolling or arm motion. This kind of motion is too weak and short to be detected by the motion target detector. Meanwhile, it corrupts the continuity of the breathing rate estimation and is missed by the stationary target detector as well. To the best of our knowledge, this is the first time that such a transition status is considered in CPD design, which contributes to about 5% improvement on the detection accuracy as validated in the experiment (see Section IV-C).

As WiCPD leverages the reflection signals from all the dynamic scatterers constructively, the motion target detector can detect motion within two consecutive CSI samples/measurements, corresponding to a shortest delay of $2\Delta t$ where $\Delta t = 1/F_s$ with F_s denoting the sample frequency. On the other hand, the MRC scheme can greatly boost the SNR of the ACF (see Fig. 5 in a later section) than simply averaging over subcarriers [45] and thus achieves 96.56% detection rate for a stationary child within 20-s while DeMan takes 3000 packets (about 100 s at 30-Hz sample rate) to detect an adult with 95% detection rate.

We have built a real-time prototype system of WiCPD using commercial NXP Wi-Fi chipsets [46], and conducted extensive experiments over 20 different cars to detect five children of different ages and genders, when the car is parked in various locations. We have also performed long-term tests to evaluate the CPU and memory consumption of the real-time WiCPD system. The results show that by only consuming 11% of a Dual-core ARM Cortex-A7 CPU up to 1 GHz and 40 MB random access memory (RAM), WiCPD achieves greater than 96.5% detection accuracy with a responsive time less than 20 s in detecting a child in vehicle regardless of his/her status.

In summary, the major contributions of WiCPD are as follows.

1) To the best of our knowledge, WiCPD is the first-of-its-kind commercial Wi-Fi-based CPD system with a high detection rate, fast responsive time, and large coverage. It can be easily incorporated in the current and future in-car Wi-Fi system with minimal installation cost as long as CSI is available[1] [31], [32].
2) We proposed a unified CPD framework consisting of three target detector modules to detect a child in all the possible status. WiCPD demonstrates $\geq$ 96.4% detection accuracy with $\leq$ 3.96% false alarm while $\leq$ 8 s to detect a child in motion and $\leq$ 20 s to detect a stationary/sleeping child.
3) We conduct extensive experiments with baby doll and real babies of different ages/genders/weights under different weather/temperature/environments. Experiments demonstrate that WiCPD can achieve accurate, robust, and responsive detection with affordable CPU and memory consumption, making it a promising candidate for world-wide deployment.

The remainder of this article is organized as follows. Section II introduces the statistical signal model. The design of WiCPD is presented in Section III followed by the implementation and evaluation in Section IV. Finally, Section V discusses the limitations and future works while Section VI concludes this article.

II. Statistical Signal Model

A. CSI on Commercial Wi-Fi

Let $X(t,f)$ and $Y(t,f)$ denote the transmitted and received signal over a subcarrier with frequency f at time t. Then, the corresponding CSI can be estimated as $H(t,f) = ([Y(t,f)]/[X(t,f)])$ [50]. Due to multipath effect, $H(t,f)$ can be expressed as follows:

$$H(t,f) = s(t,f) + n(t,f) = \sum_{l=1}^{L} \alpha_l(t,f) e^{-j2\pi f \tau_l(t)} + n(t,f) \quad (1)$$

where $s(t,f)$ denotes the channel information composed of all the propagation paths and $n(t,f)$ represents the additive white Gaussian noise (AWGN) with power density of $\sigma_n^2(f)$ at time t and frequency f. L is the number of paths, α_l and τ_l denote the complex gain and propagation delay of the lth path, respectively.

B. Statistical CSI Model

In this part, we introduce a statistical model of $s(t,f)$ in (1) based on the superposition properties of EM fields [42]. Note that the statistical model, motion statistics and using MRC to boost ACF for better breathing rate estimation are first proposed in our previous work [42], [44], [51] for indoor sensing applications. We briefly review them for completeness in this article while focusing on exploring its performance/reliability for in-vehicle environment and CPD.

[1]We note that not all the existing in-vehicle Wi-Fi chipsets/systems support direct CSI data acquisition. However, it is usually doable by minimal software modifications of the Wi-Fi driver as illustrated in the well-known Atheros CSI Tool [47] and Linux 802.11n CSI Tool [48]. In addition, the IEEE 802.11 community is now supporting the integration of wireless sensing through the IEEE 802.11bf standard, where CSI data collection and analysis will be greatly expedited [49].

Authorized licensed use limited to: University of Maryland College Park. Downloaded on November 25,2024 at 20:18:04 UTC from IEEE Xplore. Restrictions apply.

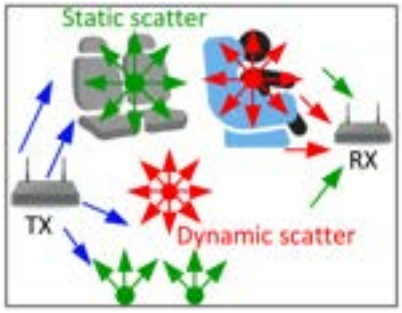

Fig. 1. Multipath propagation inside the car.

The intuition/principle of the statistical model is that each scatter can be treated as a *virtual antenna* which transmits its received EM waves in all the directions as shown in Fig. 1. These EM waves will then add up together at the received antenna after bouncing off the in-car scatterers [52]. Therefore, $s(t,f)$ can be rewritten as follows:

$$s(t,f) = \sum_{k\in\Omega_s(t)} s_k(t,f) + \sum_{m\in\Omega_d(t)} s_m(t,f) \tag{2}$$

where $\Omega_s(t)$ and $\Omega_d(t)$ denote the set of static and dynamic scatterers, respectively. $s_k(t,f)$ and $s_m(t,f)$ represent the EM waves transmitted/reflected by the kth static scatterer and the mth dynamic scatterer, respectively.

In practice, within a very short period, it is reasonable to assume that $\Omega_s(t)$ and $s_k(t,f), k \in \Omega_s(t)$ barely change. As a result, the contribution of all the static scatters can be approximated as a constant, i.e.,

$$s(t,f) \approx E_s(f) + \sum_{m\in\Omega_d(t)} s_m(t,f) \tag{3}$$

where $E_s(f) = \sum_{k\in\Omega_s(t)} s_k(t,f)$.

Given the channel reciprocity, EM waves traveling in both directions will undergo the same changes [52]. Therefore, if the receiver (RX) were transmitting EM waves, the received EM waves at the mth scatter/*virtual antenna* would be the same as $s_m(t,f)$. As a result, $s_m(t,f)$ can be expressed as follows [53]:

$$s_m(t,f) = \int_0^{2\pi}\int_0^{\pi} F_m(\Theta,f)\exp\left(-j\vec{k}\cdot\vec{v}_m t\right)\sin(\alpha)\,\mathrm{d}\alpha\,\mathrm{d}\beta \tag{4}$$

where $\vec{v}_m$ denotes the motion speed of the mth scatter. $F(\Theta)$ denotes the complex gain incoming from direction $\Theta = (\alpha,\beta)$ while α and β stand for the elevation and azimuth angles, respectively. $\vec{k} = -k(\vec{x}\sin(\alpha)\cos(\beta) + \vec{y}\sin(\alpha)\sin(\beta) + \vec{z}\cos(\alpha))$ and $k = [(2\pi f)/c]$ denote the free-space wave number with c being the speed of light.

III. WiCPD Design

This section presents the design of WiCPD, which aims at enabling accurate and responsive in-car CPD using commercial Wi-Fi. In general, we can categorize a child in the following three different status and design corresponding detector modules.

1) *Motion:* A child who is awake has frequent/substantial motions, such as swinging his/her arms/legs/torso, random body motions during his/her struggling to get out of the baby seat, etc. Usually, this kind of motion induces a large number of dynamic scatterers and can be detected by a *motion target detector*.
2) *Stationary:* A sleeping child has negligible motion. A *stationary target detector* is designed to capture the continuous breathing rate of the child and thus identify his/her presence.
3) *Transition:* A child is sleeping but with slight and intermittent motion such as occasionally moving his head during sleeping. Since this kind of motion only corresponds to the movement of a very small part of the child's body (i.e., a few dynamic scatterers), it cannot lead to a detectable change on the CSI and thus cannot be captured by the motion target detector. Yet, it will corrupt the minute breathing motion associated with the minute chest movement and fail the continuous breathing rate estimation. To handle this case, we design a *transition target detector*.

A. System Overview

Fig. 2 depicts the overview of the WiCPD system. The left side is an illustration of the in-car environment where the green dotted lines denote the multipath signal propagation inside the car. The RX measures the CSI from the incoming packets transmitted by the TX. The CSI measurements are first passed through a Hampel filter [54] to remove outliers induced by practical distortions such as jitters of the phase-locked loops (PLLs) [55]. Afterwards, the CSIs are processed by the *motion target detector* to detect if there is a child in motion inside the vehicle. If the decision is YES, WiCPD reports a "child in vehicle." Otherwise, the *stationary target detector* is triggered to detect the presence of a stationary child. If neither the *motion target detector* nor the *stationary target detector* detects the presence of a child, the *transition target detector* will further confirm if the child is in a transition status, i.e., sleeping with slight/intermittent motion. WiCPD outputs "no child in vehicle" only when neither of the three aforementioned detectors detects a child in vehicle.

To detect a child in motion in the vehicle, we leverage the statistical ACF of the Wi-Fi CSI measurements and a motion statistics metric, which constructively utilizes the reflection signal from all the dynamic scatters to reflect the instantaneous ambient motion strength of surrounding targets in motion status.

To detect a stationary child, we first leverage the motion statistics on each subcarrier to select those subcarriers which are sensitive to motions since the breathing motion corresponds a child's chest movement is subtle and easily to be submerged by the noise. Then, the motion statistics on those selected subcarriers are utilized as weights to further boost the SNR of the breathing motion in an MRC manner [44], [56]. Afterwards, the breathing rate is estimated and a "child in vehicle" is detected only when a normal breathing

Authorized licensed use limited to: University of Maryland College Park. Downloaded on November 25,2024 at 20:18:04 UTC from IEEE Xplore. Restrictions apply.

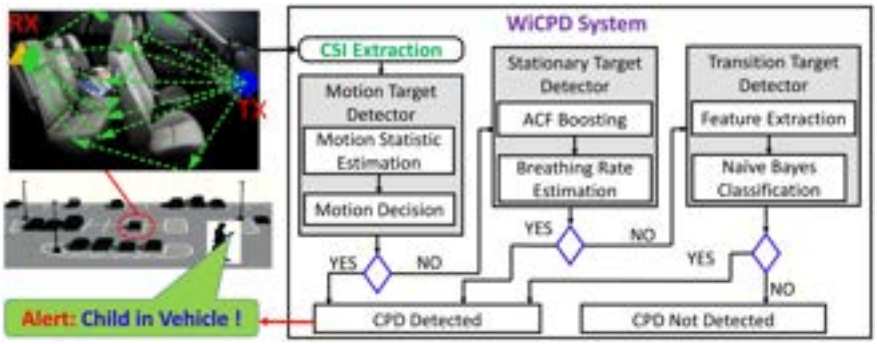

Fig. 2. System architecture of WiCPD.

rate[2] is estimated and lasts for a certain duration, since an instantaneous breathing rate may be corrupted by noise.

To detect a child in transition status, we harness the following three observations: 1) intermittent breathing rates can be estimated, even though not continuously; 2) the motion statics when a child is present is different from that in a real empty vehicle, even though it cannot be distinguished by using the motion target detection only; 3) inspired by [59], the top k largest eigenvalues of the covariance matrix $\mathbf{R}_H$ of the CSI can represent the multipath profile (more specifically, Angle of Arrival (AoA)) of the present target. Therefore, we construct a new feature using the top k largest eigenvalues of $\mathbf{R}_H$, to extract the CSI change on AoA caused by the intermittent slight motion of a child in transition status. Eventually, the motion statistics, breathing rate estimates, and top k largest eigenvalues of $\mathbf{R}_H$ form a feature vector, which is then fed into a native Bayes classifier [60] to detect if there is a child in transition status of not.

Next, we will introduce the motion target detector, stationary target detector, and transition target detector in detail.

B. Motion Target Detector

To detect a child in motion, we consider the modeling in our previous work [42], where a link between the ACF of CSI and the motion of the surrounding dynamics scatterers/objects is established, a motion statistics is defined to quantify the intensity of surrounding motions, a motion target detector is presented based on the motion statistics. However, we evaluate it in-vehicle environments.

ACF Calculation: Recalling (1), the ACF of the measured CSI is given by

$$\rho_H(\tau,f)=\frac{\mathrm{cov}\big[H(t,f),H(t+\tau,f)\big]}{\sqrt{\sigma^2_{H(t,f)}\sigma^2_{H(t+1,f)}}} \tag{5}$$

where cov[AB] denotes the covariance between A and B. $\sigma^2_{H(t,f)}$ and $\sigma^2_{H(t_\tau,f)}$ denote the variance of $H(t,f)$ and $H(t+\tau,f)$, respectively. Substituting (1) and (2) into (5), we have

$$\rho_H(\tau,f)=\frac{E_d^2(f)}{E_d^2(f)+\sigma_n^2(f)}\rho_s(\tau,f)+\frac{\sigma_n^2(f)}{E_d^2+\sigma_n^2(f)}\delta(\tau) \tag{6}$$

[2]A normal breathing rate here refers to [6, 35] beats per minute (BPM) [57], [58].

where $\delta(\cdot)$ is a Dirac delta function. $E_d^2(f)$ is the variance of $s(t,f)$ which measures the power reflected by all the dynamic scatterers. $\rho_s(\tau,f)$ can be written as follows[3]:

$$\rho_s(\tau,f)\approx\frac{1}{E_d^2(f)}\sum_{m\in\Omega_d}\sigma^2_{F_m}(f)\rho_{E_m}(\tau,f) \tag{7}$$

where $\rho_{E_m}(\tau,f)=\sum_{u\in\{x,y,z\}}\rho_{E_{m,u}}(\tau,f)$ represents the autocorrelation of the received EM field in $\{x,y,z\}$ directions and $\sigma^2_{F_m}(f)$ denotes the reflection power of the mth dynamic scatter. It can be approved that $\rho_{E_m}(\tau,f)$ is a continuous function at $\tau=0$ [52]. As a result, in (7), if there are dynamic scatters, i.e., $\sigma^2_{F_m}(f)>0$, we have $\rho_s(\tau,f)\to 1$ when $\tau\to 0$. Substituting (7) into (6), we have

$$\rho_H(\tau,f)=\frac{E_d^2(f)}{E_d^2(f)+\sigma_n^2(f)}>0,\ \text{when}\ \tau\to 0. \tag{8}$$

Otherwise, if there is no dynamic scatterer, we have $\sigma^2_{F_m}(f)=0$ and $E_d^2(f)=0$ and thus

$$\rho_H(\tau,f)=\frac{E_d^2(f)}{E_d^2(f)+\sigma_n^2(f)}=0,\ \text{when}\ \tau\to 0. \tag{9}$$

As a result, $\lim_{\tau\to 0}\rho_H(\tau,f)$ can work as a indicator of the surrounding dynamic scatters/motion targets. More importantly, the scattering power of all the dynamic scatters are added in a constructive way in (7) and thus making it more sensitive to target motions. As a preliminary verification, we collect CSI about 3 mins in a typical car with and without the presence of a motion/awake child using a pair of Wi-Fi devices with 2 Tx antennas and 2 Rx antennas, running on 5.8 GHz with 40-MHz bandwidth. Fig. 3 shows that the motion statistics behaves differently in empty and motion environments. Moreover, it has less overlap between the empty and motion case than CSI variance, thus indicating a better sensitivity of the motion statistics.

Motion Statistics: In practice, $\lim_{\tau\to 0}\rho_H(\tau,f)$ can be approximated by $\lim_{\tau\to 0}\rho_H(\tau,f)\approx\rho_H([1/(F_s)],f)$ and we average the $\lim_{\tau\to 0}\rho_H(\tau,f)$ over all the subcarriers to get a more reliable motion indicator, which is called *motion*

[3]Detailed derivations are omitted due to the space limitation while can be found in the well established statistical EM theory about the spatial correlation for fields in 3-D channels [42], [52], [53].

Authorized licensed use limited to: University of Maryland College Park. Downloaded on November 25,2024 at 20:18:04 UTC from IEEE Xplore. Restrictions apply.

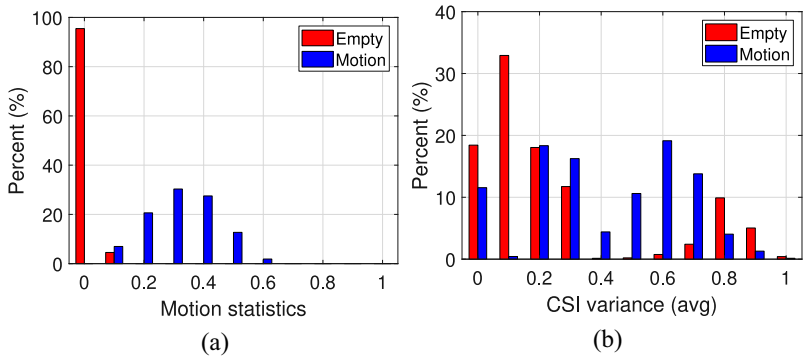

Fig. 3. Comparison between motion statistic and CSI variance in an empty car and a car with the presence of a motion/awake child.

statistics hereafter, i.e.,

$$\lim_{\tau \to 0} \rho_H(\tau, f) = \frac{1}{N_f} \sum_{i=1}^{N_f} \rho_H\left(\frac{1}{F_s}, f_i\right) \tag{10}$$

where F_s is the sample rate, N_f denotes the number of subcarriers, and f_i representing the frequency of the ith subcarrier. To avoid the motion statistics outlier due to the instantaneous distortion/noise, we use a 2 s sliding window to compute the averaged motion statistics in the practical experiments/applications.

A question is whether the motion statistic is easily to be affected by the motion/dynamic targets outside the vehicle, such as the passing cars and pedestrians. We note that the motion statistics is robust against the motion outside of the vehicle. This is because a closed vehicle can be viewed as a metal cavity which bounds most of the radio signals inside the car while shields the outside wireless/radio inferences. We show the experiment validations in Section IV-C.

Motion Target Detector: Given the motion statistics, the principle of the *motion target detector* is very straightforward, i.e., a child in a vehicle is detected when the motion statistics is larger than a threshold η_0 which is derived in the following.

When there is no motion in the car, according to (1) and (3), the CSI $H(t, f_i)$ consists of only static scattered signal $E_s(f)$ and white noise $n(t, f)$, i.e., $H(t, f_i) = E_s(f) + n(t, f)$ where $E_s(f)$ can be assumed as a constant in a empty car. As a result, given a sufficient large number of samples N_T, $\rho_H(1/F_s, f_i)$ can be approximated as a Gaussian variable with mean $1/N_T$ and variance $1/N_T$, i.e., $\rho_H(1/F_s, f_i) \sim \mathcal{N}(1/N_T, 1/N_T)$. Therefore, the distribution of the motion statistic $\hat{\rho}_H(\tau)$ in an empty car can be approximated by

$$\hat{\rho}_H(\tau) \sim \mathcal{N}\left(\frac{1}{N_T}, \frac{1}{N_T N_f}\right). \tag{11}$$

To verify the derivation in (11), we collect 1 h CSI data in an empty car using a pair of commercial Wi-Fi devices with carrier frequency $f_c = 5.805$ GHz and bandwidth with 40 MHz. Fig. 4 shows the Quantile–Quantile (Q–Q) plot of $\hat{\rho}_H(\tau)$ calculated from practical CSI measurements and the Gaussian distribution with mean $(1/N_T)$ and variance $[1/(N_T N_f)]$, which validates our derivations.

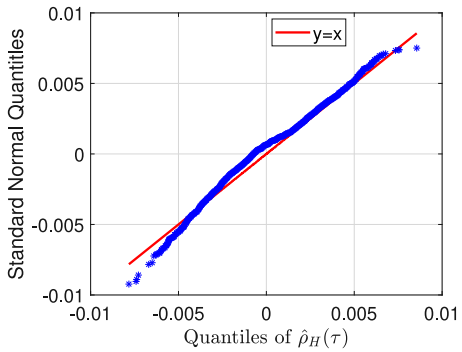

Fig. 4. Statistical distribution of $\hat{\rho}_H(\tau)$ in an empty car.

Given (11), we can derive the motion detection threshold η_0 with a predefined false alarm rate p_{F}, i.e.,

$$P\left(\hat{\rho}_H(\tau) > \eta_0\right) = p_{\mathrm{F}} \tag{12}$$

$$\Rightarrow \eta_0 = Q^{-1}(p_{\mathrm{F}}) * \frac{1}{\sqrt{N_T N_f}} + \frac{1}{N_T} \tag{13}$$

where $Q^{-1}(\cdot)$ is the inverse function of the Q-function with $Q(x) = (1/2\pi) \int_x^{\infty} \exp(-[u^2/2])\, \mathrm{d}u$.

C. Stationary Target Detector

Although existing work has shown the feasibility of estimating the breathing rate of an adult using wireless signal [41], [61], [62], estimating the breathing rate for a child can be more challenging because the size of a child is much smaller than an adult and his/her motion/breathing strength is much weaker as well. As a result, the SNR of the breathing signal of a child is very low due to the slight motion of the chest movement. To tackle the issue, we first select the subcarriers with the top N_s (default as 10) largest motion statistics,[4] aiming at extracting the subcarriers which are most sensitive to the subtle chest/breathing motion. Then, an MRC [43] scheme is leveraged to maximize the SNR of the ACF for breathing rate estimation [44]. We briefly review the main process below and readers can refer [44] for details.

[4]Here the motion statistic is computed on each subcarrier independently.

Authorized licensed use limited to: University of Maryland College Park. Downloaded on November 25,2024 at 20:18:04 UTC from IEEE Xplore. Restrictions apply.

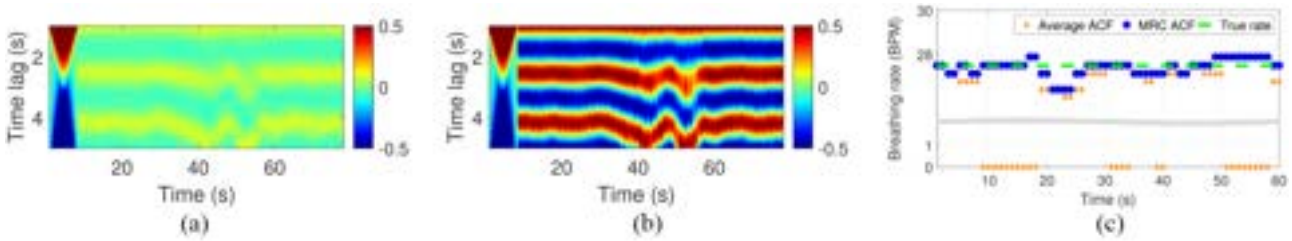

Fig. 5. Boosted ACF of the breathing signal and the corresponding breathing rate estimation. (a) Averaged ACF. (b) MRC boosted ACF. (c) Breathing rate estimation.

Considering MRC techniques, the boosted ACF can be expressed as follows:

$$\hat{\rho}_H^b(\tau) = \sum_{i=1}^{N_s} \omega(f_i)\rho_H(\tau, f_i) \tag{14}$$

where $\omega(f_i)$ is the channel gain of the breathing strength on subcarrier f_i. Recalling (6), the channel gain of subcarrier f_i in terms of ACF is $[(E_d^2(f))/(E_d^2(f) + \sigma_n^2(f))]$ which can be estimated by $\lim_{\tau\to 0} \rho_H(\tau, f_i)$ (see (7)–(9) for details). As a result, WiCPD takes $\lim_{\tau\to 0} \rho_H(\tau, f_i)$ as the optimal $\omega(f_i)$ and thus the ACF of the breathing signal can be boosted by

$$\hat{\rho}_H^b(\tau) = \sum_{i=1}^{N_f} \left[\lim_{\tau\to 0} \rho_H\left(\tau = \frac{1}{F_s}, f_i\right)\right] \rho_H(\tau, f_i). \tag{15}$$

Fig. 5 shows an example about the ACF of the CSI measurements when a baby doll is sleeping in the car with a true breathing rate of 27.5 BPM. As shown in Fig. 5(a) and (b), the MRC approach achieves about 10 dB improvement in terms of ACF compared with the existing method [45] which averages over all the subcarriers directly. As a result, the breathing rate estimated from the MRC boosted ACF is more accurate and continuous as shown in Fig. 5(c). Note that we cannot maximize the breathing signal/motion directly because that the channel gain of breathing signal cannot be directly extracted from the CSI measurements. However, this problem is circumvented by applying MRC on the ACF with the motion statistics of each subcarrier as the optimal weights.

Once we get the boosted ACF $\hat{\rho}_H^b(\tau)$, the breathing rate of the child can be estimated by $f_B = 60/\hat{\tau}$(BPM) where $\hat{\tau}$ corresponds to the time lag of the first peak in $\hat{\rho}_H^b(\tau)$. Afterwards, the *stationary target detector* reports a child in vehicle if a normal child breathing rate (i.e., within [6, 35] BPM) is detected and continuously lasts for a certain duration.

D. Transition Target Detector

If neither the previous *motion target detector* nor the *stationary target detector* detects "a child in vehicle," the *transition target detector* is triggered.

A child in transition status can induce a certain level of motion statistics and intermittent breathing rate estimation, which exhibits a different pattern from a real empty vehicle, even though they cannot be detected by the *motion target detector* or the *stationary target detector* only. To detect the presence of a target in transition status, we consider the fact that the slight/intermittent motion of a child can change the AoAs of partial of the multipath signals. Even though such a change cannot be used to estimate the AoAs of the target directly, it is inherently embedded in the measured CSI and can be leveraged as a new feature. We resort to extracting the intermittent motion information using the top k largest eigenvalues of the covariance matrix $\mathbf{R}_H$ of the CSI [59] and construct a feature vector containing the motion statistic, breathing rate, and the top k largest eigenvalues of $\mathbf{R}_H$. All these features are fused together in a Naive Bayes classifier. We omit the details of the Naive Bayes classifier and readers can refer to [59].

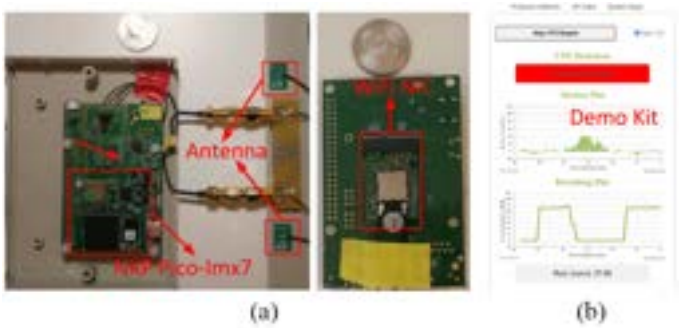

Fig. 6. Experiment platform of WiCPD. (a) Hardware. (b) Software.

IV. Evaluation

To comprehensively evaluate WiCPD, we build a real-time system using the commercial Wi-Fi chipsets and conduct extensive experiments in various car models to validate the CPD detection performance using real babies and baby dolls.

A. Methodology

Implementation: As shown in Fig. 6(a), we build the hardware system using the commercial NXP Wi-Fi chipset which is dual-band operating on both 2.4 and 5 GHz. To get CSI, we modify the driver of the Wi-Fi chipset. The main processing board is a PICO-IMX7 System-on-Module consisting of a Dual-core ARM Cortex-A7 CPU up to 1 GHz. The Wi-Fi chipset contains two antennas with U.FL/IPX connector interfaces that can conveniently connect to the external PCB antennas or the on-car antennas. The RX receives packets transmitted from the TX and captures CSI, containing 58 subcarriers with a sample rate of 30 Hz, unless otherwise mentioned. Both the TX and RX consist of two omnidirectional

Authorized licensed use limited to: University of Maryland College Park. Downloaded on November 25,2024 at 20:18:04 UTC from IEEE Xplore. Restrictions apply.

PCB antennas. The system runs on the 5.805-GHz channel (default U.S. channel 161) with a bandwidth of 40 MHz.

We first develop the algorithm and the real-time system using MATLAB for performance analysis and validation. It is then implemented using C++ and ported on the PICO-IMX7 board running on the Linux system. To display the CPD estimation results, we develop a Demo Kit using Python, which shows the live motion statistic, breathing rate estimations, and the CPD detection results as shown in Fig. 6(b). During the real-time experiment, the RX keeps capturing CSI and running the WiCPD algorithm to calculate the corresponding CPD decision, which is then sent to the Demo Kit via Wi-Fi every 1 s.

Data Collection: The data collection mainly involves three parts, including 1) empty case over 20 different cars in different scenarios; 2) experiments for the Lifelike Ashley baby doll; and 3) experiments with real babies. As the cars are usually empty for most of the time, we perform an extensive evaluation of false alerts by gathering data from over 20 different cars. For the baby doll test, we deploy WiCPD in four different family cars[5,6]. For each car, the TX is first located in the center of the dash board and then in the glove box as shown in Fig. 7. RX is mounted in four different locations, including three on the car liner next to top of rear car seat and 1 in the cup holder of the rear door.[7] As shown in Fig. 7, in total we have eight TX-RX configurations and two categories of testing objects including: *1) Baby Doll:* In total, 11 different locations inside the car are tested using the baby doll as an object. Specifically, the baby doll sits in a standard car seat [see Fig. 7(a)] in location #3, #4, #9, #10, and #11 while it is put in the footwell area with no car seat[8] in location #1, #2, #5, #6, #7, and #8 to mimic the case that the child falls down from the car seat.[9] At each location, when the baby doll sits in a car seat, it is tested with forward and rear-facing direction, respectively. Moreover, three different postures, including lying on the floor facing up, facing down, and sitting on the floor are tested when the baby doll is in the footwell area. *2) Real Baby:* We also evaluate the performance of WiCPD in detecting five real babies of different ages and genders as shown in Table II. Overall, our experiments range from a four months infant to a five years toddler with different heights and weights. During the test, the baby sits in the car seat with buckled up in location #3, #4, #9 #10, and #11. We do not test the footwell area because of its limited spaces to put the car seat in. TX is placed at location #1 while the two antennas of the RX are separately mounted in location #1 and #3 to harvest the best coverage.

[5]The test cars include a Toyota Camry SE Sedan of size 192″L × 72.4″W × 56.9″H, a Toyota Highlander of size 197″L × 76″W × 68″H, a Honda HR-V Hatchback of size 169″L × 70″W × 63″H, and a Honda Civic Sedan of size 182″L × 71″W × 56″H. The Toyota Highlander has three rows of car seats while the others have two rows of car seats

[6]*L* stands for length, *W* stands for width while *H* stands for height. All are in inches denoted by symbol″.

[7]The locations of the TX and RX are the favored locations for car antennas according to our survey with the original equipment manufacturers (OEMs) and car manufactures.

[8]The space is too small to put a car seat in.

[9]For example, Maryland U.S. current law requires that children under eight years old to ride in an appropriate child restraint, unless the child is 4′9" or taller.

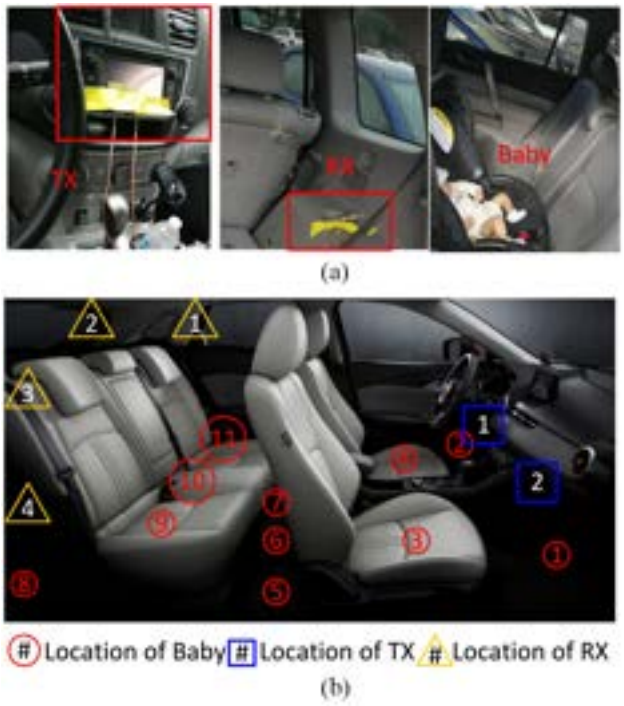

Fig. 7. Experiment scenarios. Eleven different locations of the baby, two different locations of the TX, and four different RX locations are tested. Note that baby/child in locations #1, #2, #5, #6, and #7 represent the footwell area while #8 represents the trunk area for hatchback cars. TX in #1 is fixed in the center of the dashboard while it is put inside the glove box in location #2. RX in #1, #2, and #3 are on the car liner next to the top of the car seats while location #4 denotes the cup holder on the rear door. (a) Example of the experiment setup. (b) Test scenarios in a typical car.

TABLE II
OBJECT BABY OF WICPD EXPERIMENT

#	Age (Month)	Gender	Height (inch)	Weight (lbs)
1	4	Male	25	16.07
2	6	Female	-	-
3	20	Male	32.9	24
4	36	Male	-	-
5	58	Female	44.4	43

The experiments are conducted over different days across 13 months in different environments, including an outdoor parking lot next to a trade center, a underground garage of a shopping mall, street parking, and a personal garage for family use. The in-car environment has natural changes as the car owner uses the car on a daily basis. Note that the in-car environment is allowed to freely change without any restrictions during this time. WiCPD is a calibration-free system in different real-world environments without any impractical assumptions/constraints.

B. Overall Accuracy

To evaluate the overall performance of WiCPD, three key metrics, including responsive time, detection rate, and false

Authorized licensed use limited to: University of Maryland College Park. Downloaded on November 25,2024 at 20:18:04 UTC from IEEE Xplore. Restrictions apply.

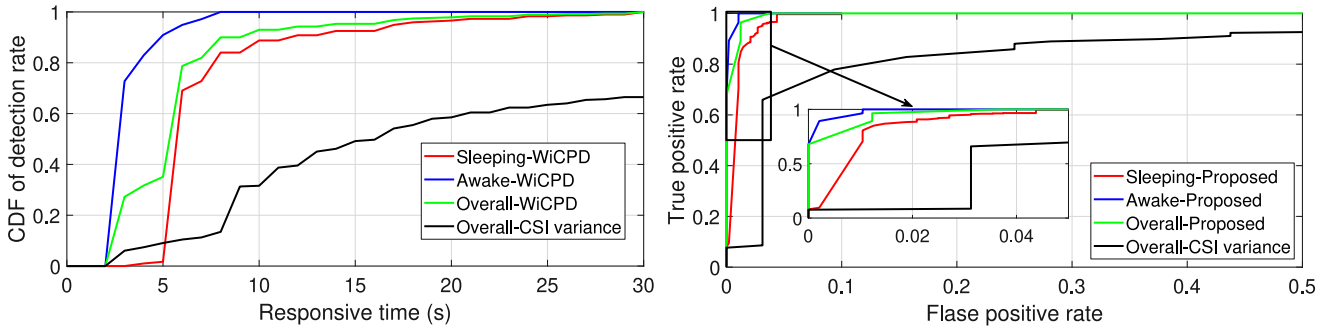

Fig. 8. Overall performance of WiCPD system. (a) Detection rate. (b) ROC curves.

alarm rate[10] are demonstrated since they are the key requirements to detect/rescue a child left alone in the vehicle timely. Note that we do not evaluate the performance of detecting a child in transition status independently because the transition status is usually merged with the sleeping/stationary status. Hereafter, "Sleeping" refers to a stationary child in sleeping while "Awake" means the child is awake and more likely to create motions.

Fig. 8 shows that WiCPD achieves 100% detection rate with less than 8 s responsive time for an awake child in motion with normal activities such as struggling to get out of the car. Besides, WiCPD shows 96.56% detection rate within 20 s for a sleeping child. As shown in Fig. 8(a), WiCPD takes a slightly longer responsive time to detect a sleeping child. This is because that the stationary target detector takes at least more than one breathing cycling time to estimate the breathing rate and thus causing a longer delay. However, Fig. 8 shows that overall WiCPD can still achieve more than 97.87% detection rate with the response time less than 20 s, which is a quite secure time for CPD applications. Fig. 8(c) shows the Receiver's operating characteristic curve (ROC) of WiCPD, indicating 1.04% and 3.96% false alarm rate for an awake and sleeping child, respectively, with the detection rate $\geq$ 96.4%.

C. Comparison With Existing Works

We also implement a benchmark method (named as "Overall-CSI variance" in Fig. 8) in which we replace the *motion target detector* module with the*CSI variance-based motion detector* [40] and exclude the *transition target detector*. As seen in Fig. 8, WiCPD outperforms the benchmark methods in all the responsive time, detection rate, and false alarm rate mainly because:

1) *Robust Motion Target Detector:* on the one hand, WiCPD leverages a motion statistic based on a statistical EM model considering all the multipath components. Thus, it enjoys better sensitivity to the surrounding motions than that based on CSI variance, as shown in Section III-B and Fig. 3. On the other hand, WiCPD also enjoys very robust performance to the motions outside the car since a closed car can be regarded as a closed metal box which can separate the inside and outside wireless/radio signals very well. To verify, we conduct empty data collection in eight different scenarios, i.e., a) an empty car in an outdoor parking lot with no motion target around; b) there are cars driving around, for example passing through the adjacent parking space; c) pedestrians walking around an empty car; d) an empty car in the garage; e) empty car in windy weather; f) an empty car in street parking with cars passing by once in a while; g) outdoor parking lot; and h) in a rainy weather. As seen in Fig. 9(a), over 99.29% of the motion statistics are less than 0.1 for outside motions and 94.4% of the in-car motions demonstrate larger than 0.1 motion statistics. However, the CSI variance shows a much larger overlap between the in-car and outside motions as shown in Fig. 9(b). Therefore, WiCPD is not only good at capturing surrounding motions but also resilient against the motion outside the car and thus promising it as a robust solution in practice;
2) *Powerful Stationary Target Detector:* WiCPD utilizes the motion statistics as channel gain to first select those subcarriers which are sensitive to breathing motion and then combine them in an MRC way. As a result, WiCPD can greatly boost the SNR of the breathing motion embedded in the ACF (see Fig. 5) and achieves more accurate and responsive estimation of breathing rate to capture the static child inside the car;
3) *Novel Transition Target Detector:* to handle the experimentally observed missing cases[11] by both the *motion target detector* and *stationary target detector*, a Naive Bayes classifier based *transition target detector* is proposed, which, to the best of our knowledge, was never considered in the existing works. To test the contribution of the transition detector independently, we only use the real baby data and exclude the data from the babydoll. This is mainly because that the baby doll is usually either static or in-motion and lacks such a transition status that only exists in a real child.[12] Table III demonstrates the performance of CPD with

[10]Detection rate is also known as true positive rate and false alarm rate is also known as false positive rate.

[11]Few of the existing works have mentioned such a case and it may be due to that they have never been tested under such a comprehensive test.

[12]From our experiment there are about 6.5% of the time during which a sleeping child is in transition status.

Authorized licensed use limited to: University of Maryland College Park. Downloaded on November 25,2024 at 20:18:04 UTC from IEEE Xplore. Restrictions apply.

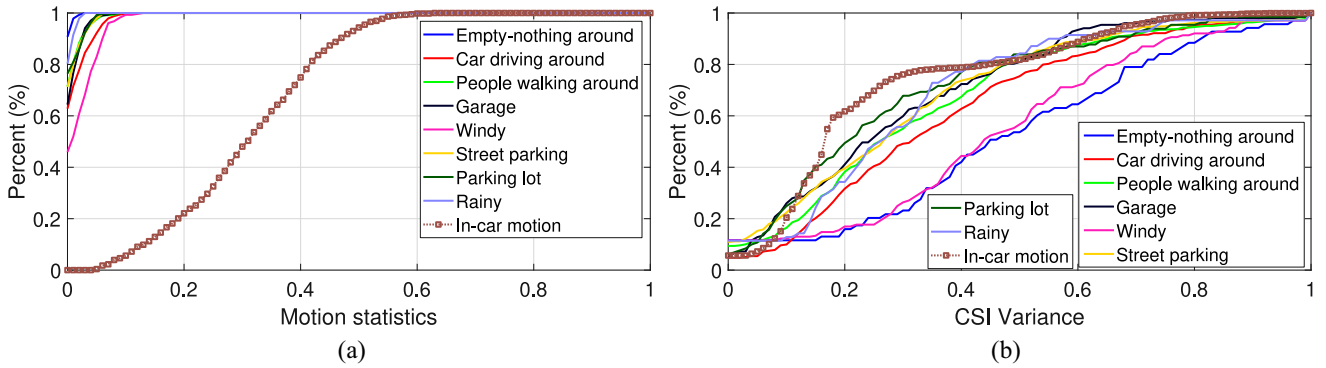

Fig. 9. Motion statistics versus CSI variance: in an empty car or with the presence of an motion/awake child in a car. (a) CDF of detection using motion statisitcs. (b) CDF of detection using the variance of CSI.

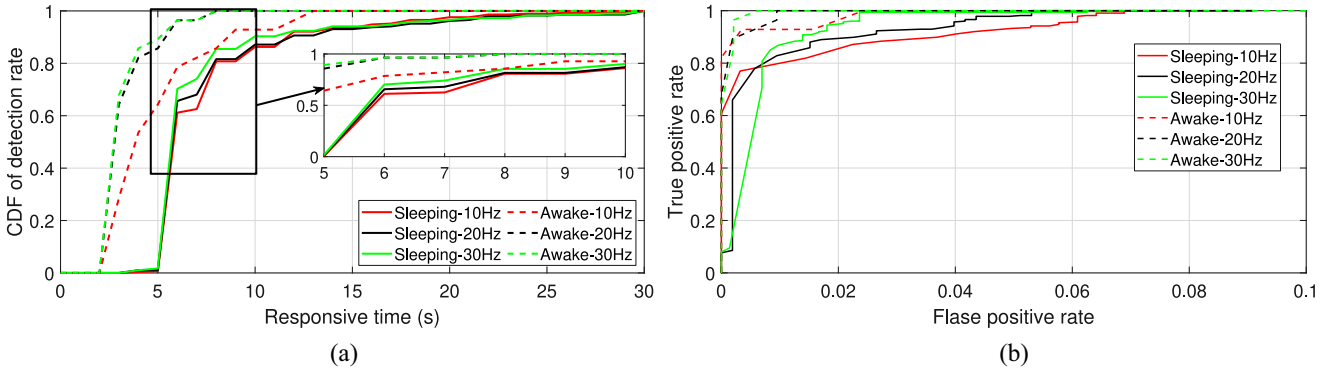

Fig. 10. Performance of WiCPD versus sample rate F_s. (a) Detection rate. (b) ROC curves.

TABLE III
EVALUATION ON THE TRANSITION TARGET DETECTOR

CPD without transition detector		CPD with transition detector, i.e., **WiCPD**	
TP[1]	FP[2]	TP	FP
93.1%	1.14%	**98.6%**	**1.79%**

[1] True Positive Rate (TP), a.k.a. detection rate.
[2] False Positive Rate (FP), a.k.a. false alarm rate.

versus without the transition target detector. As seen, WiCPD improves about 5.5% detection rate by incorporating the transition target detector with a moderate of 0.65% increment in false alarm rate.

D. Impact of Sample Rate

As shown in Section III-B, a higher sample rate F_s can provide WiCPD with better motion statistic and breathing estimations, thus improving the overall performance. However, in practice, a higher sample rate will increase the overhead of the hardware system and may cause interference to the surrounding Wi-Fi network. As a result, we evaluate the performance with different sample rates, which can guide the practical settings. Fig. 10(a) shows that WiCPD takes 13, 8, and 8 s response time to achieve 100% detection accuracy for the detection of an awake child, corresponding to the sample rate of 10, 20, and 30 Hz. Additionally, it achieves $\geq$ 96.18% detection rate with a responsive time of 20 s for all the 10, 20, and 30 Hz cases in detecting a static child. Note that in practice, CPD system should consider detection rate first since every missing case may be catastrophic. As a result, we recommend $F_s = 30$ Hz, which is affordable for most of the Wi-Fi systems.

E. Impact of Effective Bandwidth

We study the impact of the effective bandwidth attributed by antennas and bandwidth together. Specifically, the effective bandwidth N_e is defined as $N_e = N_s B$ where $N_s = N_{\text{TX}} \cdot N_{\text{RX}}$ denoting the spatial links between TX and RX with N_{TX} and N_{RX} representing the number of TX and RX. B is the bandwidth of the Wi-Fi system which is 40 MHz for 5 GHz channel and 20 MHz for 2.4 GHz channel in the WiCPD system. Fig. 11(a) shows that when detecting an awake child with the responsive time set as 8 s, WiCPD achieves 85.46%, 92.86%, and 100% detection rate with the effective bandwidth increased from 40 up to 160 MHz. In the presence of a sleeping child, the detection rate increases from 75.62% to 86.68% when N_e goes from 40 to 160 MHz, corresponding to a responsive time of 8 s as well. As shown in Fig. 11, the responding sensitivity and false alarm rate are also improved with the increment of effective bandwidth. Overall, Fig. 11 depicts that WiCPD can achieve a remarkable performance by using the typical 2×2 Wi-Fi system with 40 MHz bandwidth.

Authorized licensed use limited to: University of Maryland College Park. Downloaded on November 25,2024 at 20:18:04 UTC from IEEE Xplore. Restrictions apply.

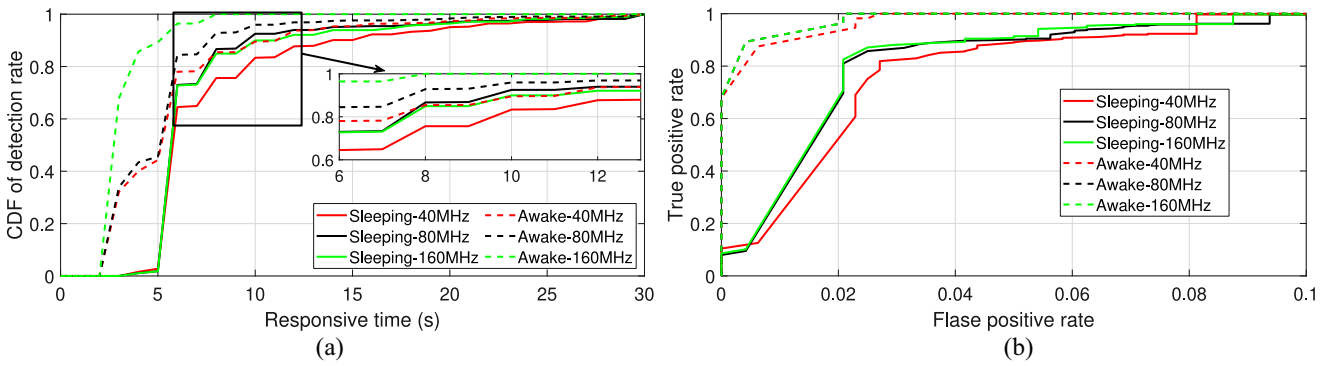

Fig. 11. Performance of WiCPD versus bandwidth N_e. (a) Detection rate. (b) ROC curves.

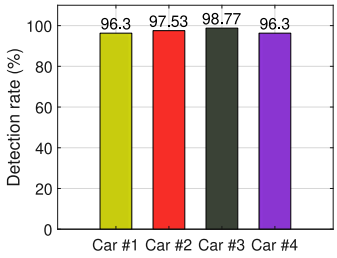

Fig. 12. Verification for different cars (see Section IV-F for details of the car models).

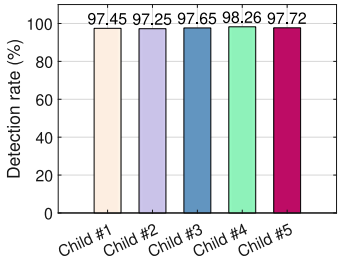

Fig. 13. Verification for different children (from young to old, Table II).

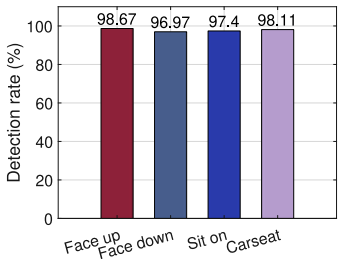

Fig. 14. Verification for different postures of the children (in or our of the carseat).

F. Environment Independence

To be a world-wide CPD system, it is important to evaluate its robustness in different environments, such as in different cars, children of different ages, and genders. As a result, this section evaluates the detection rate of WiCPD in the following aspects: 1) different car models; 2) different children; 3) different postures of the children; and 4) different commercial antennas operating on different central frequencies and bands.

Independence on Different Cars: Fig. 12 shows the detection rate of WiCPD in four different car models including: a Toyota Highlander (Car #1), a Toyota Camry SE Sedan (Car #2), a Honda HR-V Hatchback (Car #3), and a Honda Civic Sedan (Car #3). As seen, WiCPD achieves larger than 96.3% detection rate with marginal differences less than 2.47% among different cars. The slight differences in performance are mainly because different cars own different materials, structures, and sizes. Different size will cause different propagation path lengths/losses of the wireless signal and thus inducing differences on the received energy $E_d^2(f)$ [see (6)] bounced off the dynamic scatterers. On the other hand, cars of different materials/structures have different impacts on reflecting the in-car signal and shielding the out-car signal as well.

Independence on Different Children: As the children suffer from being left alone in a car can age from newborns to six years old [2], we now evaluate the performance of WiCPD in detection children over different ages and genders. As shown in Table II, we recruit five children aging from four months to four years and ten months old with the permissions from their parents. Fig. 13 demonstrates that WiCPD can successfully detect different children with at least 97.25% detection rate. The detection rate among different children slightly deviates with a maximum of 1.01%, which shows the great ability of WiCPD to detect child presence regardless of ages and genders.

Independence on Different Postures: We study the impact of the postures since a child may demonstrate different postures in practice. Different from the existing works which use adults to mimic child for posture control convenience, we use the baby doll instead. The reason is that adults have larger body size and stronger chest movement than that of the babies. As a result, the received energy $E_d^2(f)$ (see (6)) reflected from a baby and an adult is quite different. In Fig. 14, the *face up, face down, and sit on* postures correspond to the data collected by a baby doll while the *carseat* is captured from a real baby who sits in a car seat by law. As shown in Fig. 14, WiCPD achieves larger than 96.97% for all the postures and thus facilitates the deployment of WiCPD in practical applications.

Independence on Different Antennas: Fig. 15 evaluates the detection performance of WiCPD over different commercial antennas operating in both 2.4 and 5 GHz bands, which is to examine its potential to integrate with different cars

Authorized licensed use limited to: University of Maryland College Park. Downloaded on November 25,2024 at 20:18:04 UTC from IEEE Xplore. Restrictions apply.

TABLE IV
COMPUTATIONAL COMPLEXITY

Method		Complexity	Example (CMs)
WiCPD	Motion target detector	$O\{(2N_sN_f-1)(T_{\mathrm{M}}f_s-1)\}$	2.561×10^4
	Stationary target detector	$O\{[(2T_{\mathrm{B}}-T_P+4N_sN_f)f_s+1](T_{\mathrm{P}}f_s)/2\}$	3.398×10^6
	Transition target detector	$O\{T_{\mathrm{T}}f_sN_sN_f+(N_sN_f)^3+2(2+K)\}$	1.250×10^7

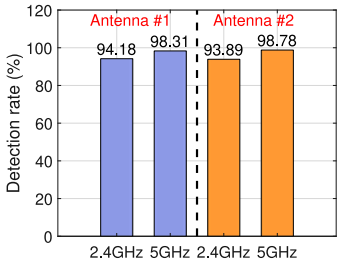

Fig. 15. Verification for different physical antennas and carrier frequency.

equipped with different antennas. As seen, WiCPD achieves up to 98.13% and 98.78% by using antenna[13] #1 and #2 centered on 5 GHz, receptively. Overall, WiCPD shows comparable performance (i.e., within 0.5% difference in detection rate) for the two different antennas in both 2.4 and 5G systems. As a result, Fig. 15 sheds light on WiCPD deployment on a variety of cars with different antennas, if integrated properly. Moreover, WiCPD is promising to improve its performance by harvesting more effective bandwidth with the increment of antennas and bandwith in the future, yet not available at present.

G. System Overhead

Aiming at practical applications, it is interesting to evaluate the system overhead in different aspects. Toward this end, we analyze both the theoretical computation complexity and resource consumption of WiCPD in real-time experiments. To measure the real-time resource consumption, we conduct long-term experiments in four different cars and carry out two experiments for each car with a duration of 30 mins for each trial. A baby doll is used to mimic the trapped child and a toy car (remote control) is adopted to cause motion once a while. Here, we choose baby doll for two main reasons: 1) leaving a child in a closed car for such a long time would cause serious damages to his/her health and thus is prohibited and 2) our goal to is evaluate the system latency and consumption which has nothing to do with the tested object. During the test, we keep track of the resource consumption by saving the log provided by *top*[14] command in the Linux system. It is worthwhile to note that WiCPD can be set up in minutes when deployed in a new car thanks to its elegant calibration-free feature.

[13]Antenna #1 is the TE 2118309-1 dual-band Wi-Fi PCB antennas and Antenna #2 is from the car manufacture for future on car Wi-Fi system which is anonymized for privacy concerns.

[14]*Top* command is typically used to show a dynamic real-time view of the running Linux system, including the usage of CPU, memory, etc., with a default updating rate of every 3 s.

Computational Complexity: Recalling that N_s denotes the spatial links between TX and RX while N_f denotes the number of subcarriers, Table IV summaries the computational complexity of the three detectors in WiCPD. T_{M} and T_{B} represent the time window length to estimate the motion statistics and breathing rate, respectively. T_{P} denotes the length of time lag covering the first local peak of ACF to estimate the breathing rate and T_{T} is the time window length to calculate the covariance matrix for eigenvalue estimation. To have a better understanding, Table IV includes a typical example of the computation complexity with $T_{\mathrm{M}}=T_{\mathrm{T}}=2$ s, $T_{\mathrm{B}}=12$ s, $T_{\mathrm{P}}=8$ s, $N_s=4$, $N_f=58$, $f_s=30$, and $K=10$. Note that the computational complexity is calculated in terms of the number of complex multiplication operations (CMs). As seen in Table IV, the stationary and transition target detector take much more computational resource than that of the motion target detector. However, WiCPD detects the motion target, stationary target, and transitional target in a cascaded way, thus minimizing the resource consumption in practice.

Resource Consumption: Fig. 16 shows a 10-mins snapshot of the real-time result and Fig. 17 demonstrates the resource consumption of WiCPD in terms of CPU and memory running on a Dual-core ARM Cortex-A7 CPU up to 1-GHz Linux on the board system. As seen, WiCPD responds timely to the alternation between motion and stationary situations and achieves robust CPD detection results with a consumption of only about 11% of the CPU and 40-MB RAM. Note that the consumption of CPU and RAM can be further reduced in practice where we only transmit the necessary binary CPD detection decision while do not involve a GUI as shown in Fig. 6, thus saving more resources.

H. Comparative Study

Although we have compared WiCPD with the benchmark algorithm in Section IV-B, we would like to compare with more exiting CPD systems [4]–[16], [20]–[25], [63] as summarized in Table I. Yet, few of them have been tested under such extensive conditions since most of them are patents [4]–[7], [11], [63], on-line demos [21]–[25] which focus on methodology and proof of concept verification. As a result, we briefly categorize the existing work as Sensor-CPD [4]–[10], PIR Motion-CPD [11]–[13], [63], Vision-CPD [14]–[16], Radar-CPD [20]–[25], and compare with them from technical aspects.

Sensor-CPD: Sensor-CPD methods usually equip physical sensors on the baby seat, such as weight sensor to detect weight [4], [5], RFID sensors to detect electrical continuity [7], or the distance between the caregiver and the baby seat [8].

Authorized licensed use limited to: University of Maryland College Park. Downloaded on November 25,2024 at 20:18:04 UTC from IEEE Xplore. Restrictions apply.

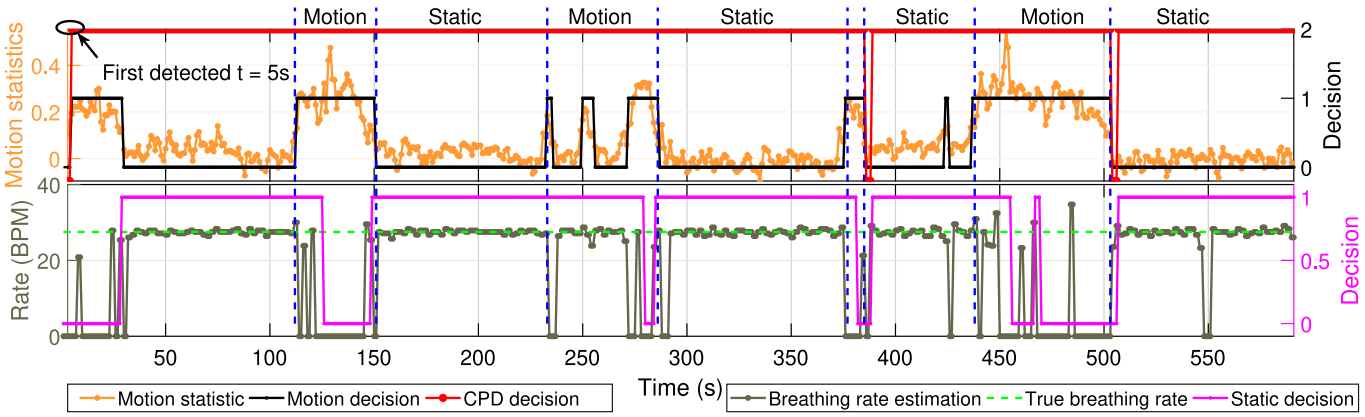

Fig. 16. 10-mins snapshot of the real-time test.

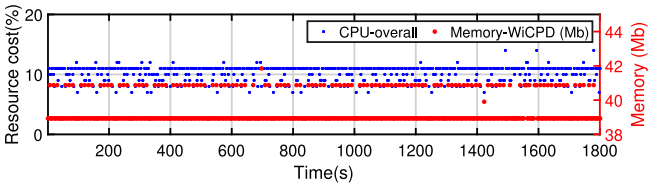

Fig. 17. Resource consumption of WiCPD in a real-time experiment of 30 mins.

Recent works also use captive sensors to detect the capacitance between the child body and nearby capacitive sensors [9], [10] and moreover, the fusion of multiple sensors [6]. While most of them work well in detecting the child on the baby seat, they suffer from high false alarm rates since a weight/pressure sensor cannot distinguish a child with an inanimate item as long as they are of the same weight. In addition, their sensing areas are limited next to the baby seat which cannot handle the case if the child falls into the footwell area. However, WiCPD can cover the entire car space due to its statistical CSI model.

PIR Motion-CPD: PIR Motion-CPD uses infrared sensors to sense the motion [11]–[13] caused by the child and thus broads the sensing coverage than traditional Sensor-CPD. Despite of its prevalence, it is vulnerable to the surrounding temperatures since it actually detects the temperature of a warm human body within LoS areas. In this sense, WiCPD outperforms PIR Motion-CPD since it is environment independent and covers both LoS and NLoS areas.

Vision-CPD: Vision-CPD methods first capture the interior image [14]–[16] of a car using a dedicated camera and then leverage image processing to perform CPD. They are very accurate especially when combined with the popular machine learning driven image processing techniques [17]. However, they call for dedicated camera and good light condition to get high-quality images and thus prevent its practical applications. WiCPD greatly eases the task by leveraging the on car Wi-Fi system regardless of the light conditions.

Radar-CPD: Radar-based methods detect the micro motion, such as vital motion (i.e., breathing and heart rate motion) as a indicator of CPD. Recent works also demonstrate potential CPD candidates using mmWave radars operating on 24, 60, 69, and 79 GHz [21]–[25]. They demonstrate surprising high accuracy when the target is within the FoV of the radar, by leveraging the high directionality, angular, and range resolution of mmWave signal due to its high central frequency. However, there are two sides to every coin. High frequency also results in rapid signal propagation attenuation and high directionality makes the mmWave system more sensitive to the location/posture of the child [20]. While mmWave is very encouraging, it is not yet to integrate with current on the car Wi-Fi system (most on 2.4 and 5 GHz) without additional hardware cost. On the contrary, WiCPD shows better potential in combination with the existing on the car Wi-Fi system with almost zero additional hardware cost.

V. Discussions and Future Works

A. Multiple Children Presence Detection

Currently, WiCPD mainly demonstrates the presence detection performance of a single child. However, it can be easily extended to multiple children scenarios for the following reasons. First, by leveraging motion statistics, WiCPD can detect the motion of all the dynamic scatters in a constructive way. In this sense, WiCPD is better at capturing the motion of multiple children and thus reporting CPD detection since multiple children are more likely to induce motion than a single child. When there are multiple children under stationary status in the car, the ACF of the CSI will be dominated by the breathing signal of the child who has the strongest breathing motion/displacement. Hence, the stationary target detector of WiCPD can still estimate and check the continuity/duration of the estimated breathing rate to determine CPD. Similarly, multiple children in transition status trapped in the car will change the multipath profile inside the car, which can be detected by the transition detector as well.

B. Future Work

While WiCPD focuses on the CPD, the statistical modeling accounting for all the multipath components inspires new opportunities for Wi-Fi sensing-based in-car applications. First, a direct extension can be in-car vital sign monitoring based on the estimated breathing rate. Driver's vital sign can be further leveraged to analyze the behavior of a driver, such as fatigue and inattentive driving, which we believe

Authorized licensed use limited to: University of Maryland College Park. Downloaded on November 25,2024 at 20:18:04 UTC from IEEE Xplore. Restrictions apply.

can expedite the popular ADAS research. Nevertheless, monitoring a driver's behavior is more challenging due to the vibrations during driving while WiCPD targets at a parked vehicle. However, recent works [64], [65] have shown the possibility to detect/compensate/suppress the unwanted motions such as by detrending techniques. Second, if we can estimate the breathing rates for both the driver and passengers during driving, it can be prior information to further reduce the responsive time of WiCPD. Third, occupancy detection (a.k.a. in car passenger counting) may be enabled using Wi-Fi sensing since the received CSI can be regarded as the superposition of the breathing signals coming from different individuals, if any. Consequently, the recently proposed decomposition techniques, such as variational mode decomposition (VMD) [66] and multivariate VMD (MVMD) [67] can be applied to estimate the mode of the signal and thus indicating the number of people in a car.

VI. Conclusion

This article presents the design, implementation, and evaluation of WiCPD, a novel CPD using CSI measurements extracted from commercial Wi-Fi chipsets. We leverage a statistical EM theoretical modeling to account for the impact of a target to all the multipath components. Then, three detector modules are designed to enable WiCPD regardless of the child's status, including motion, stationary, and transition in between. We implement the system using commercial Wi-Fi chipsets and deploy it in different cars to detect different children of different ages and genders. Extensive results show that WiCPD can achieve $\geq 96.5\%$ accuracy with a responsive time less than 20 s. The real-time tests show that WiCPD runs with affordable computational overhead, making it a promising candidate for world-wide CPD applications.

References

[1] M. Catherine, N. Jan, and Q. James, "Heat stress from enclosed vehicles: Moderate ambient temperatures cause significant temperature rise in enclosed vehicles," *Pediatrics*, vol. 116, no. 1, pp. e109–e112, 2005.

[2] "Heatstroke deaths of children in vehicles." [Online]. Available: https://www.noheatstroke.org/original/ (Accessed: Mar. 6, 2021).

[3] "Euro NCAP 2025 roadmap." [Online]. Available: https://cdn.euroncap.com/media/30700/euroncap-roadmap-2025-v4.pdf (Accessed: Mar. 6, 2021).

[4] A. R. Marc, "Warning system for detecting presence of a child in an infant seat," U.S. Patent 5 949 340, Sep. 1999.

[5] J. C. Charles, "System to detect the presence of an unattended child in a vehicle," U.S. Patent 7 170 401, Jan. 2007.

[6] L. Davis, "Child carseat alert system," U.S. Patent 7 250 869, Jul. 2007.

[7] J. K. Lee, D. R. Spach, P. Srinivasan, and D. P. Umstead, "Wireless system to detect presence of child in a baby car seat," U.S. Patent 7 321 306, Jan. 2008.

[8] K. N. Khamil, S. Rahman, and M. Gambilok, "Babycare alert system for prevention of child left in a parked vehicle," *ARPN J. Eng. Appl. Sci.*, vol. 10, no. 22, pp. 17313–17319, 2015.

[9] J. Albesa and M. Gasulla, "Occupancy and belt detection in removable vehicle seats via inductive power transmission," *IEEE Trans. Veh. Technol.*, vol. 64, no. 8, pp. 3392–3401, Aug. 2015.

[10] A. Ranjan and B. George, "A child-left-behind warning system based on capacitive sensing principle," in *Proc. IEEE Int. Instrum. Meas. Technol. Conf. (I2MTC)*, 2013, pp. 702–706.

[11] F. R. M. Rashidi and I. H. Muhamad, "Vehicle's interior movement detection and notification system," *Recent Adv. Autom. Control Model. Simulat.*, vol. 2013, pp. 139–144, Apr. 2013. [Online]. Available: https://www.safetylit.org/citations/index.php?fuseaction=citations.viewdetails&citationIds[]=citjournalarticle_493561_26

[12] P. Zappi, E. Farella, and L. Benini, "Tracking motion direction and distance with pyroelectric IR sensors," *IEEE Sensors J.*, vol. 10, no. 9, pp. 1486–1494, Sep. 2010.

[13] N. Hashim, H. Basri, A. Jaafar, M. Aziz, and A. S. A. Ja, "Child in car alarm system using various sensors," *ARPN J. Eng. Appl. Sci.*, vol. 9, no. 9, pp. 1653–1658, 2014.

[14] M. I. Hafiz and F. R. M. Rashidi, "In-car suffocating prevention using image motion detection," in *Proc. SCOPORO*, 2013, p. 12.

[15] H. Cai, D. Lee, H. Joonkoo, Y. Fang, S. Li, and H. Liu, "Embedded vision based automotive interior intrusion detection system," in *Proc. IEEE Int. Conf. Syst. Man Cybern. (SMC)*, 2017, pp. 2909–2914.

[16] C. Fan, Y. Wang, and C. Huang, "Heterogeneous information fusion and visualization for a large-scale intelligent video surveillance system," *IEEE Trans. Syst., Man, Cybern., Syst.*, vol. 47, no. 4, pp. 593–604, Apr. 2017.

[17] J. Redmon and A. Farhadi, "Yolov3: An incremental improvement," 2018, *arXiv:1804.02767*.

[18] F. Wang, X. Zeng, C. Wu, B. Wang, and K. J. R. Liu, "mmHRV: Contactless heart rate variability monitoring using millimeter-wave radio," *IEEE Internet Things J.*, vol. 8, no. 22, pp. 16623–16636, Nov. 2021.

[19] F. Wang, X. Zeng, C. Wu, B. Wang, and K. J. R. Liu, "Driver vital signs monitoring using millimeter wave radio," *IEEE Internet Things J.*, vol. 9, no. 13, pp. 11283–11298, Jul. 2022.

[20] A. Caddemi and E. Cardillo, "Automotive anti-abandon systems: A millimeter-wave radar sensor for the detection of child presence," in *Proc. 14th Int. Conf. Adv. Technol. Syst. Services Telecommun. (TELSIKS)*, 2019, pp. 94–97.

[21] Vayyar Inc. "Testing with all ages of infants in various child seats." [Online]. Available: https://vayyar.com/auto/(Accessed: Mar. 6, 2021).

[22] Novelic Inc. "NOVELIC radar automotive in-cabin monitoring." [Online]. Available: https://www.novelic.com/radar-solutions/(Accessed: Mar. 6, 2021).

[23] Infineon Inc. "Presece detection." [Online]. Available: https://www.infineon.com/cms/en/applications/solutions/sensor-solutions/presence-detection/(Accessed: Mar. 6, 2021).

[24] Innosent Inc. "Child presence detection with RADAR—Anonymous vehicle interior monitoring." [Online]. Available: https://www.innosent.de/en/automotive/incabin-radar-monitoring/ (Accessed: Mar. 6, 2021).

[25] IEE-Sensing, Inc. "Sensing solutions for child presence detection." [Online]. Available: https://www.iee-sensing.com/en/automotive/safety-and-comfort/vitasense(Accessed: Mar. 6, 2021).

[26] B. Wang, Q. Xu, C. Chen, F. Zhang, and K. J. R. Liu, "The promise of radio Analytics: A future paradigm of wireless positioning, tracking, and sensing," *IEEE Signal Process. Mag.*, vol. 35, no. 3, pp. 59–80, May 2018.

[27] K. R. Liu and B. Wang, *Wireless AI: Wireless Sensing, Positioning, IoT, and Communications*. Cambridge, U.K.: Cambridge Univ. Press, 2019.

[28] B. Schleicher, I. Nasr, A. Trasser, and H. Schumacher, "IR-UWB radar demonstrator for ultra-fine movement detection and vital-sign monitoring," *IEEE Trans. Microw. Theory Techn.*, vol. 61, no. 5, pp. 2076–2085, May 2013.

[29] "Hot and cold: Extreme temperature safety." [Online]. Available: https://www.healthline.com/health/extreme-temperature-safety#extreme-heat-temperatures(Accessed: Aug. 12, 2021).

[30] "Connected cars worldwide—Statistics & facts." [Online]. Available: https://www.statista.com/topics/1918/connected-cars/#topicHeader__wrapper (Accessed: Jun. 19, 2022).

[31] "Cheap cars with WiFi capability." [Online]. Available: https://www.autobytel.com/car-buying-guides/features/cheap-cars-with-wifi-capability-130477/ (Accessed: Mar. 6, 2021).

[32] Car and Driver Research. "Cars with Wi-Fi: Everything you need to know." [Online]. Available: https://www.caranddriver.com/research/a32814112/cars-with-wifi/ (Accessed: Mar. 6, 2021).

[33] "How many connected cars are sold worldwide?" [Online]. Available: https://smartcar.com/blog/connected-cars-worldwide/(Accessed: Jun. 19, 2022).

[34] "Projected share of new Internet-connected light-duty vehicles sales worldwide and in the United States in 2023." [Online]. Available: https://www.statista.com/statistics/275849/number-of-vehicles-connected-to-the-internet/ (Accessed: Jun. 19, 2022).

Authorized licensed use limited to: University of Maryland College Park. Downloaded on November 25,2024 at 20:18:04 UTC from IEEE Xplore. Restrictions apply.

[35] X. Xie, K. G. Shin, H. Yousefi, and S. He, "Wireless CSI-based head tracking in the driver seat," in *Proc. 14th Int. Conf. Emerg. Netw. Exp. Technol.*, 2018, pp. 112–125.
[36] M. Raja and S. Sigg, "RFexpress! Exploiting the wireless network edge for RF-based emotion sensing," in *Proc. 22nd IEEE Int. Conf. Emerg. Technol. Factory Autom. (ETFA)*, 2017, pp. 1–8.
[37] X. Zeng, F. Wang, B. Wang, C. Wu, K. J. R. Liu, and O. C. Au, "In-vehicle sensing for smart cars," *IEEE Open J. Veh. Technol.*, vol. 3, pp. 221–242, 2022.
[38] X. Zeng, B. Wang, W. Chenshu, S. D. Regani, and K. J. R. Liu, "Intelligent Wi-Fi based child presence detection system," in *Proc. ICASSP IEEE Int. Conf. Acoust. Speech Signal Process. (ICASSP)*, 2022, pp. 11–15.
[39] Q. Xu, B. Wang, F. Zhang, D. S. Regani, F. Wang, and K. J. R. Liu, "Wireless AI in smart car: How smart a car can be?" *IEEE Access*, vol. 8, pp. 55091–55112, 2020.
[40] Y. Gu, J. Zhan, Y. Ji, J. Li, F. Ren, and S. Gao, "MoSense: An RF-based motion detection system via off-the-shelf WiFi devices," *IEEE Internet Things J.*, vol. 4, no. 6, pp. 2326–2341, Dec. 2017.
[41] C. Wu, Z. Yang, Z. Zhou, X. Liu, Y. Liu, and J. Cao, "Non-invasive detection of moving and stationary human with WiFi," *IEEE J. Sel. Areas Commun.*, vol. 33, no. 11, pp. 2329–2342, Nov. 2015.
[42] F. Zhang, C. Wu, B. Wang, H. Q. Lai, Y. Han, and K. J. R. Liu, "WiDetect: Robust motion detection with a statistical electromagnetic model," *Proc. ACM Interact. Mobile Wearable Ubiquitous Technol.*, vol. 3, no. 3, pp. 1–24, 2019.
[43] E. A Lee and D. G. Messerschmitt, *Digital Communication*. New York, NY, USA: Springer, 2012.
[44] F. Zhang *et al.*, "SMARS: Sleep monitoring via ambient radio signals," *IEEE Trans. Mobile Comput.*, vol. 20, no. 1, pp. 217–231, Jan. 2021.
[45] J. Liu, Y. Wang, Y. Chen, J. Yang, X. Chen, and J. Cheng, "Tracking vital signs during sleep leveraging off-the-shelf WiFi," in *Proc. 16th ACM Int. Symp. Mobile Ad Hoc Netw. Comput.*, 2015, pp. 267–276.
[46] "NXP S32 automotive platform." [Online]. Available: https://www.nxp.com/products/processors-and-microcontrollers/s32-automotive-platform:S32 (Accessed: Jun. 19, 2022).
[47] "Atheros CSI tool." [Online]. Available: https://wands.sg/research/wifi/AtherosCSI/(Accessed: Jun. 19, 2022).
[48] "Linux 802.11n CSI tool." [Online]. Available: https://dhalperi.github.io/linux-80211n-csitool/ (Accessed: Jun. 19, 2022).
[49] F. Restuccia. "IEEE 802.11 BF: Toward ubiquitous Wi-Fi sensing." 2021. [Online]. Available: https://dhalperi.github.io/linux-80211n-csitool/(Accessed: Jun. 19, 2022).
[50] T. Chiueh, P. T. I. Lai, and T. Chiueh, *Baseband Receiver Design for Wireless MIMO-OFDM Communications*. Hoboken, NJ, USA: Wiley, 2012.
[51] F. Zhang, C. Chen, B. Wang, and K. J. R. Liu, "WiSpeed: A statistical electromagnetic approach for device-free indoor speed estimation," *IEEE Internet Things J.*, vol. 5, no. 3, pp. 2163–2177, Jun. 2018.
[52] D. A. Hill, *Electromagnetic Fields in Cavities: Deterministic and Statistical Theories*, vol. 35. Hoboken, NJ, USA: Wiley, 2009.
[53] D. A. Hill, "Plane wave integral representation for fields in reverberation chambers," *IEEE Trans. Electromagn. Compat.*, vol. 40, no. 3, pp. 209–217, Aug. 1998.
[54] R. K. Pearson, Y. Neuvo, J. Astola, and M. Gabbouj, "Generalized hampel filters," *EURASIP J. Adv. Signal Process.*, vol. 2016, no. 1, pp. 1–18, 2016. [Online]. Available: https://doi.org/10.1186/s13634-016-0383-6
[55] Y. Xie, Z. Li, and M. Li, "Precise power delay profiling with commodity Wi-Fi," *IEEE Trans. Mobile Comput.*, vol. 18, no. 6, pp. 1342–1355, Jan. 2019.
[56] L. Kahn, "Correspondence," *Proc. IRE*, vol. 42, no. 11, pp. 1698–1704, 1954.
[57] G. Shafiq and K. C. Veluvolu, 1 "Surface chest motion decomposition for cardiovascular monitoring," *Sci. Rep.*, vol. 4, no. 1, pp. 1–9, 2014.
[58] L. A. Wallis, M. Healy, M. Undy, and I. Maconochie, "Age related reference ranges for respiration rate and heart rate from 4 to 16 years," *Arch. Disease Childhood*, vol. 90, no. 11, pp. 1117–1121, 2005.
[59] S. Fang, R. Alterovitz, and S. Nirjon, "Non-line-of-sight around the corner human presence detection using commodity WiFi devices," in *Proc. 1st ACM Int. Workshop Device Free Human Sens.*, 2019, pp. 22–26.
[60] S. Di Domenico, M. De Sanctis, E. Cianca, and M. Ruggieri, "WiFi-based through-the-wall presence detection of stationary and moving humans analyzing the doppler spectrum," *IEEE Aerosp. Electron. Syst. Mag.*, vol. 33, nos. 5–6, pp. 14–19, May/Jun. 2018.
[61] F. Wang, F. Zhang, C. Wu, B. Wang, and K. J. R. Liu, "Respiration tracking for people counting and recognition," *IEEE Internet Things J.*, vol. 7, no. 6, pp. 5233–5245, Jun. 2020.
[62] C. Chen *et al.*, "TR-BREATH: Time-reversal breathing rate estimation and detection," *IEEE Trans. Biomed. Eng.*, vol. 65, no. 3, pp. 489–501, Mar. 2018.
[63] M. Hansjürg, R. Martin, and A. Rolf, "Presence detector and its application," U.S. Patent 6 486 778, Nov. 2002.
[64] C. Ding *et al.*, "Inattentive driving Behavior detection based on portable FMCW radar," *IEEE Trans. Microw. Theory Techn.*, vol. 67, no. 10, pp. 4031–4041, Oct. 2019.
[65] T. Zheng, Z. C. C. Cai, J. Luo, and X. Zhang, "V2iFi: In-vehicle vital sign monitoring via compact RF sensing," *Proc. ACM Interact. Mobile Wearable Ubiquitous Technol.*, vol. 4, no. 2, pp. 1–27, 2020.
[66] K. Dragomiretskiy and D. Zosso, "Variational mode decomposition," *IEEE Trans. Signal Process.*, vol. 62, no. 3, pp. 531–544, Nov. 2014.
[67] N. U. Rehman and H. Aftab, "Multivariate variational mode decomposition," *IEEE Trans. Signal Process.*, vol. 67, no. 23, pp. 6039–6052, Dec. 2019.

Xiaolu Zeng received the B.S. degree from Harbin Institute of Technology, Harbin, China, in 2014, and the Ph.D. degree from the School of Electronic Engineering, Xidian University, Xi'an, Chin, in 2020.

He is currently an Assistant professor with the School of Information and Electronics, Beijing Institute of Technology, Beijing, China. He was a Postdoctoral Research Associate from July 2020 to December 2021, and a visiting student from September 2017 to June 2020, with the Department of Electrical and Computer Engineering, University of Maryland, College Park, MD, USA. His research interests include intelligent wireless sensing, Internet of Things, and advanced driver assistance systems.

Beibei Wang (Senior Member, IEEE) received the B.S. degree in electrical engineering (Hons.) from the University of Science and Technology of China, Hefei, China, in 2004, and the Ph.D. degree in electrical engineering from the University of Maryland, College Park, MD, USA, in 2009.

She was with the University of Maryland as a Research Associate from 2009 to 2010, and with Qualcomm Research and Development, San Diego, CA, USA, from 2010 to 2014. Since 2015, she has been with Origin Wireless Inc., Greenbelt, MD, USA, where she is currently the Vice President of Research. She has coauthored *Cognitive Radio Networking and Security: A Game-Theoretic View* (Cambridge University Press, 2010) and WIRELESS AI: WIRELESS SENSING, POSITIONING, IOT, AND COMMUNICATIONS (Cambridge University Press, 2019). Her research interests include Internet of Things, mobile computing, wireless sensing, and positioning.

Dr. Wang is a recipient of the 2020 IEEE INTERNET OF THINGS JOURNAL Best Paper Award, the 2015 IEEE Signal Processing Society Overview Paper Award, and several research and invention awards from the University of Maryland. She has served on the editorial board of IEEE SIGNAL PROCESSING LETTERS, IEEE INTERNET OF THINGS JOURNAL, and IEEE JOURNAL ON SELECTED AREAS IN COMMUNICATIONS.

Chenshu Wu (Senior Member, IEEE) received the B.E. degree from the School of Software from Tsinghua University, Beijing, China, in 2010, and the Ph.D. degree in computer science from Tsinghua University in 2015.

He is currently an Assistant Professor with the Department of Computer Science, The University of Hong Kong, Hong Kong. He is also the Chief Scientist with Origin Wireless Inc., Greenbelt, MD, USA. His research focuses on wireless AIoT systems at the intersection of wireless sensing, ubiquitous computing, digital health, and the Internet of Things.

Authorized licensed use limited to: University of Maryland College Park. Downloaded on November 25,2024 at 20:18:04 UTC from IEEE Xplore. Restrictions apply.

Sai Deepika Regani received the B.Tech. degree in electrical engineering from the Indian Institute of Technology Madras, Chennai, India, in 2015, and the M.S. and Ph.D. degrees from the Department of Electrical and Computer Engineering, University of Maryland, College Park, MD, USA, in 2017 and 2021, respectively.

She is currently the Principal Scientist with Origin Wireless Inc., Greenbelt, MD, USA. Her research interests include wireless sensing, signal processing, machine learning, and deep learning.

K. J. Ray Liu (Fellow, IEEE) is the Founder and the President of Origin AI that pioneers AI for wireless sensing and indoor tracking. He was a Distinguished University Professor, a Distinguished Scholar-Teacher, and a Christine Kim Eminent Professor of Information Technology with the University of Maryland at College Park, College Park, MD, USA, from where he retired after over three decades of career in education. His research contributions encompass broad aspects of signal processing and communications. He has trained over 70 doctoral/postdoctoral students, of which ten are now IEEE Fellows.

Dr. Liu is the recipient of two IEEE Technical Field Awards: the 2021 IEEE Fourier for Signal Processing and the 2016 IEEE Leon K. Kirchmayer Graduate Teaching Award. He also received the IEEE Signal Processing Society 2014 Norbert Wiener Society Award and 2009 Claude Shannon-Harry Nyquist Technical Achievement Award. Recognized as a Web of Science Highly Cited Researcher. The invention of wireless AI won three prestigious CES Innovation Awards, including the CES Best of Innovation in 2021. He is a Fellow of the American Association for the Advancement of Science (AAAS) and the U.S. National Academy of Inventors. He is the 2022 IEEE President and the CEO. He was the 2019 IEEE Vice President for Technical Activities. He has also served as the 2012–2013 President of IEEE Signal Processing Society, where he once served as the Editor-in-Chief of *IEEE Signal Processing Magazine*.

Authorized licensed use limited to: University of Maryland College Park. Downloaded on November 25,2024 at 20:18:04 UTC from IEEE Xplore. Restrictions apply.